Journal of ELECTRONIC MATERIALS, Vol. 42, No. 12, 2013
DOI: 10.1007/s11664-013-2715-8


# Preparation of Uncapped $CdSe_xTe_{1-x}$ Nanocrystals with Strong Near-IR Tunable Absorption

SHAOHUA LI,[1] GUOLONG TAN,[1] JAMES B. MUROWCHICK,[2] CLARISSA WISNER,[3] NICKOLAS LEVENTIS,[3] TING XIA,[1] XIAOBO CHEN,[1] and ZHONGHUA PENG[1,4]

1.—Department of Chemistry, University of Missouri-Kansas City, Kansas City, MO 64110, USA. 2.—Department of Geosciences, University of Missouri-Kansas City, Kansas City, MO 64110, USA. 3.—Department of Chemistry, Missouri University of Science & Technology, Rolla, MO 65409, USA. 4.—e-mail: pengz@umkc.edu

Semiconducting nanocrystals with near-infrared (NIR) photosensitivity are appealing materials for application as photodetectors and in medical diagnostics. Herein, we report the preparation of composition-tunable, uncapped $CdSe_xTe_{1-x}$ ($x$ = 0 to 1) nanocrystals by simple mechanical alloying. The resulting ternary $CdSe_xTe_{1-x}$ ($x$ = 0.25, 0.5, 0.75) nanocrystals with average sizes smaller than 10 nm have zincblende crystal structure, instead of the wurtzite structure commonly obtained by wet chemical routes, and show strong NIR absorption even beyond 1400 nm. While a linear relationship between the lattice parameter and the chemical composition (Se/Te ratio) is observed, indicating the formation of homogeneous alloys, the bandgap energy of the three ternary samples is found to be substantially lower than that of binary CdSe or CdTe nanocrystals, and lower than any ternary CdSeTe reported so far. Existence of a small number of tellurium metal defects in the $CdSe_xTe_{1-x}$ ($x$ = 0.25, 0.5, 0.75) nanocrystals is confirmed by x-ray diffraction and Raman spectroscopy. Both the optical bowing effect and tellurium metal-induced defects of the mechanically alloyed samples are believed to cause the strong NIR photosensitivity.

**Key words:** Semiconducting nanocrystals, mechanical alloy, near-IR absorption, cadmium selenide telluride

## INTRODUCTION

Semiconducting nanocrystals (NCs) or quantum dots (QDs) exhibit attractive size- and composition-dependent optical properties which make them promising materials for application in bioimaging,[1–3] solar energy conversion,[4–7] photocatalysis,[8,9] and light-emitting diodes.[10–12] Although a large number of semiconducting NCs have been reported with absorption and emission wavelength ranges covering the ultraviolet (UV) to visible spectrum,[13–17] less attention has been paid to the near-infrared (NIR) range.[18–22] The NIR photosensitivity of QDs is an appealing and desired feature for applications in biological imaging/labeling.[21,22] It is known that light within the biological NIR window (650 nm to 900 nm), when compared with UV–visible (UV–Vis) light, can penetrate deeper through biological tissues due to less absorption and scattering by tissue constituents.[23–25] NCs with NIR absorption/emission can thus potentially be used as biodetectors or fluorescent probes in biological and medical examinations and diagnostics. While there have been a few attempts to fabricate various pure and alloyed NIR-absorbing/emitting NCs such as PbSe QDs,[26,27] HgS QDs,[28] $M_xWO_3$ (M = Na, Cs, Tl, Rb) nanoparticles,[29] and $InAs_xP_{1-x}$/InP/ZnSe alloyed core–shell QDs,[3] most attention has focused on cadmium telluride (CdTe) and its alloyed compounds. CdTe has a bandgap of only 1.44 eV, which is considerably lower than that of CdS (2.42 eV) or

(Received January 31, 2013; accepted July 29, 2013; published online August 30, 2013)

CdSe (1.74 eV).[30] By doping or by alloying with proper elements, the bandgap of the resulting alloyed QDs could be further lowered.[31,32] These QDs are usually prepared by solution-based wet chemical routes, which lead to capped QDs with impressive control on the size, shape, and size distribution.

The wet chemical approach to alloyed NCs, however, has some drawbacks: The process requires careful control of reaction temperature and reaction time, and it is difficult to scale up; the resulting alloyed NCs may lack composition homogeneity due to varied reactivity and/or solubility of the competing components; the as-prepared NCs are ligand-capped, which is beneficial for luminescence properties but may be detrimental for applications involving charge transfer in and/or out of the nanoparticles, as the capping agents are often insulating organic materials.[33] As a complementary synthetic approach, mechanical alloying [or high-energy ball milling (HEBM)] is attractive because it is easily scalable, allows facile composition tuning, and leads to homogeneous nanoparticles without capping groups.[34,35] A number of semiconducting NCs, such as PbS,[36] CdSe,[37] CdTe,[38] and ZnS,[39] have been prepared by HEBM with average sizes smaller than 10 nm. In our previous report,[40] we showed that uncapped homogeneous ternary $CdSe_{1-x}S_x$ ($x$ = 0 to 1) semiconducting NCs could be conveniently prepared by HEBM. In this contribution, we extend the HEBM approach to preparation of $CdSe_xTe_{1-x}$ ($x$ = 0 to 1) NCs. Unlike wet chemical routes which produce ternary CdSeTe with wurtzite-type structure, HEBM leads to CdSeTe NCs with zincblende structure. More interestingly and surprisingly, the mechanically alloyed CdSeTe NCs show strong NIR absorption even beyond 1400 nm, indicating a bandgap not only far smaller than that of the two binary CdSe and CdTe systems but also substantially lower than that of CdSeTe systems prepared by any wet chemical or hydrothermal route.

## EXPERIMENTAL PROCEDURES

The ball-milling reaction was conducted using a SPEX 8000 M mixer/mill. High-purity cadmium (99.99%), tellurium (99.99%), and selenium (99.99%) powders were purchased from Alfa Aesar and used without any further treatment. In a typical process, a raw powder mixture of 15 g total weight with desired atomic ratios was placed into a stainless-steel vial together with stainless milling balls (diameters 4 mm to 12 mm) in a glovebox. The powder-to-ball mass ratio was set to be 1:10. The vial was then sealed and subjected to ball milling. At different time intervals, a small amount of sample was taken out of the vial for structural and property characterizations. Crystal structure characterizations were carried out by x-ray diffraction (XRD) measurements on a Rigaku Miniflex powder x-ray diffractometer (Cu $K_\alpha$, 35 kV, 15 mA, Ni filter), and high-resolution transmission electronic microscopy (HRTEM, JEOL 2100F) was used to record TEM images. Raman spectra were collected on an EZRaman-N benchtop Raman spectrometer (Enwave Optronics, Inc., Irvine, CA). The excitation wavelength was set at 785 nm with a 300-mW diode laser.

## RESULTS AND DISCUSSION

### Structural Evolution During Mechanical Alloying

X-ray diffraction patterns of the set of samples removed at different time intervals during the mechanical alloying of Cd + 0.5Se + 0.5Te are shown in Fig. 1. Elemental diffraction peaks, such as lattice planes (002), (100), (101), and (102) of cadmium crystals and (101) of tellurium crystals dominate the spectrum of the 15 min ball-milled sample (Fig. 1a). As the mechanical alloying process continued, those elemental peaks decreased in intensity and eventually disappeared after 5 h of ball milling, indicating completion of the mechanochemical reaction Cd + 0.5Se + 0.5Te $\rightarrow$ $CdSe_{0.5}Te_{0.5}$. In the meantime, diffraction peaks corresponding to the (111), (220), and (311) lattice planes of $CdSe_{0.5}Te_{0.5}$ compound with zincblende structure appeared. The $CdSe_{0.5}Te_{0.5}$ samples ball milled for 40 h showed a good x-ray diffraction spectrum with all the major diffraction peaks being assigned to the lattice planes (111), (220), and (311) of cubic (zincblende) structure. The estimated size for the 40 h as-milled samples is ~9 nm.

Figure 2 shows the XRD patterns of $CdSe_xTe_{1-x}$ NCs with different mole ratios of Se to Te, all ball milled for 40 h. The XRD peaks are normalized with

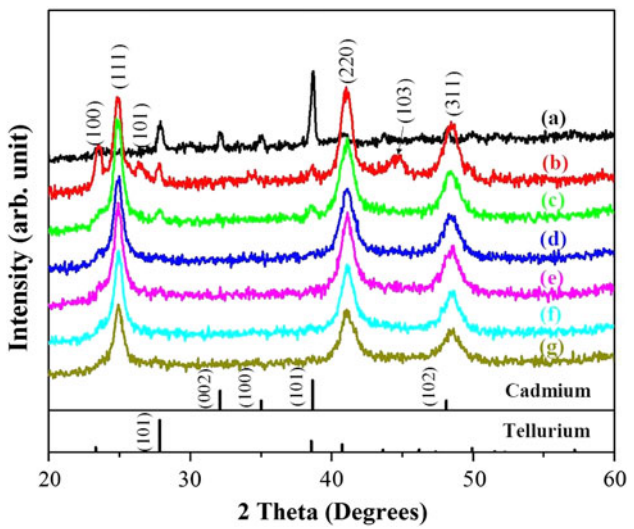


Fig. 1. XRD patterns of as-milled $CdSe_{0.5}Te_{0.5}$ products after (a) 15 min, (b) 30 min, (c) 1 h, (d) 5 h, (e) 10 h, (f) 20 h, and (g) 40 h of ball milling. The XRD patterns of elemental Cd (ICCD PDF#00-005-0674) and Te (ICCD PDF#00-036-1452) crystals are also shown for comparison.

respect to the (111) peak intensity. All samples show prominent XRD patterns of the zincblende structure with continuous lattice contraction as the molar ratio of Se in the $CdSe_xTe_{1-x}$ compounds increases. A linear relationship is found between the lattice spacing and the chemical composition (Fig. 2b), indicating that Vegard's law is followed and the formation of homogeneous alloys instead of heterogeneous mixtures of separate CdSe and CdTe NCs, in which case a superposition of the peaks of pure CdSe and pure CdTe would be expected. Using CdSe and CdTe as end members, the Te compositions in the three alloys were calculated from the x-ray diffraction peaks[41] to be in the ranges 0.77 to 0.83, 0.48 to 0.56, and 0.18 to 0.26 for $CdSe_{0.25}Te_{0.75}$, $CdSe_{0.5}Te_{0.5}$, and $CdSe_{0.75}Te_{0.25}$, respectively, which are reasonably close to the initial element loading ratios.

It should be noted that a small but clear peak at $2\theta \approx 26°$, believed to be due to (101) plane diffraction by elemental Te crystals, is observed for the $CdSe_{0.25}Te_{0.75}$, $CdSe_{0.5}Te_{0.5}$, and $CdSe_{0.75}Te_{0.25}$ samples. This peak appears at the same position for all three ternary samples, and its intensity increases in the prior compound order.

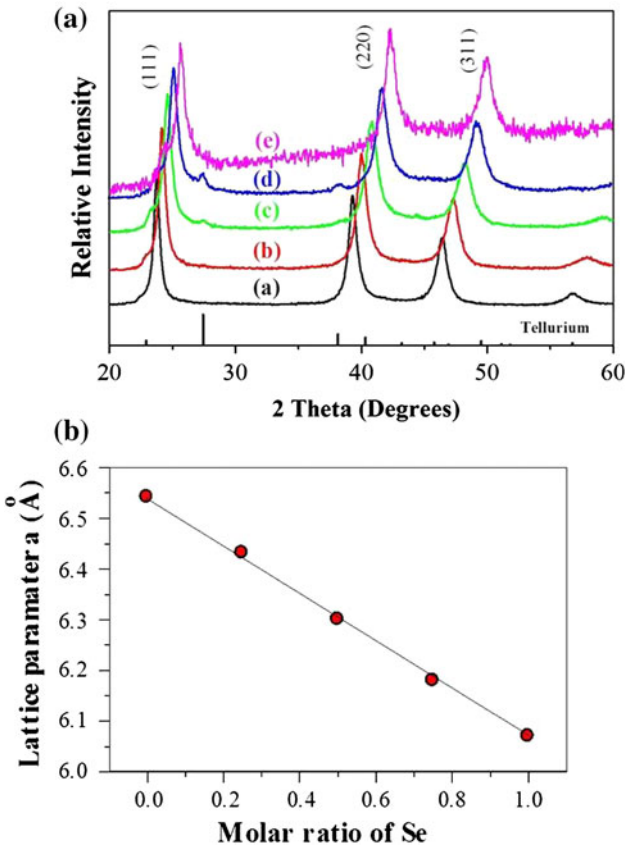


Fig. 2. (a) X-ray diffraction patterns of 40 h ball-milled $CdSe_xTe_{1-x}$ nanocrystals, where $x = 0$ (a), 0.25 (b), 0.5 (c), 0.75 (d), and 1 (e); (b) lattice parameter versus mole fraction of selenium in $CdSe_xTe_{1-x}$ nanocrystals.

## Microstructure of the Uncapped $CdTe_{0.5}Se_{0.5}$ Nanocrystals

Nanocrystals prepared by mechanical alloying tend to aggregate together to form larger particles. The repeated fracturing and welding processes of the particles trapped during collisions in ball milling cause aggregation of the particles. Nanometer grains are single crystalline, while the aggregated larger particles are polycrystalline. HRTEM images can often provide such morphological views of aggregated nanoparticles, which are composed of NC grains. Unless specifically mentioned, the following discussion on identification of the structure for the as-milled $CdTe_{0.5}Se_{0.5}$ NCs focuses on such individual NC grains, which are embedded within aggregated larger particles. Figure 3 shows HRTEM images of as-milled $CdSe_{0.5}Te_{0.5}$ NCs dispersed in ethanol by sonication. Even though most of the as-milled NCs tend to aggregate together, one can still easily pick out small individual NCs, marked by red circles, with sizes of 3 nm to 8 nm. Both images share the same scale bar. It can be seen that the small particle in the inset image of Fig. 3 exhibits only one-dimensional lattice fringes of the {111} lattice plane, the structure of which is assigned to be face-centered cubic (fcc) zincblende. The one-dimensional lattice fringes of other particles can be assigned to the {111} lattice plane of $CdSe_{0.5}Te_{0.5}$ NCs with zincblende structure as well, consistent with the conclusion drawn from XRD diffraction patterns.

Figure 4 shows HRTEM images of aggregated $CdSe_{0.5}Te_{0.5}$ NCs. The majority of the NCs have sizes within the range 2 nm to 8 nm, while a small number of aggregated particles with size around 30 nm are also observed. Fast Fourier transformation (FFT) of several individual NCs was carried out to identify the crystalline structure of the $CdSe_{0.5}Te_{0.5}$ NCs as well as the phase composition. The inset images in Fig. 4 demonstrate fast Fourier transformation of three individual NCs marked as A, B, and C. These FFT images show the structural features of individual NCs in reciprocal space. Each spot in an FFT image (reciprocal space) corresponds to one lattice plane in real space. The index of each lattice plane corresponding to the diffraction spot is labeled in these FFT images. Lattice fringes of {111}, {200} or {131} can be clearly seen in the images. Particles A, B, and C were all determined to have zincblende (cubic) structure in [011] orientation based on their FFT images in reciprocal space.

## Optical Studies of Uncapped $CdSe_xTe_{1-x}$ Nanocrystals with Various Compositions

The absorption spectra of the as-milled uncapped NCs were measured using a Shimadzu UV-3600 UV–Vis-NIR spectrophotometer with an ISR3100 integrating sphere attachment which allows direct measurement of powder samples. Figure 5 shows the UV–Vis–NIR spectra of the alloyed $CdSe_xTe_{1-x}$

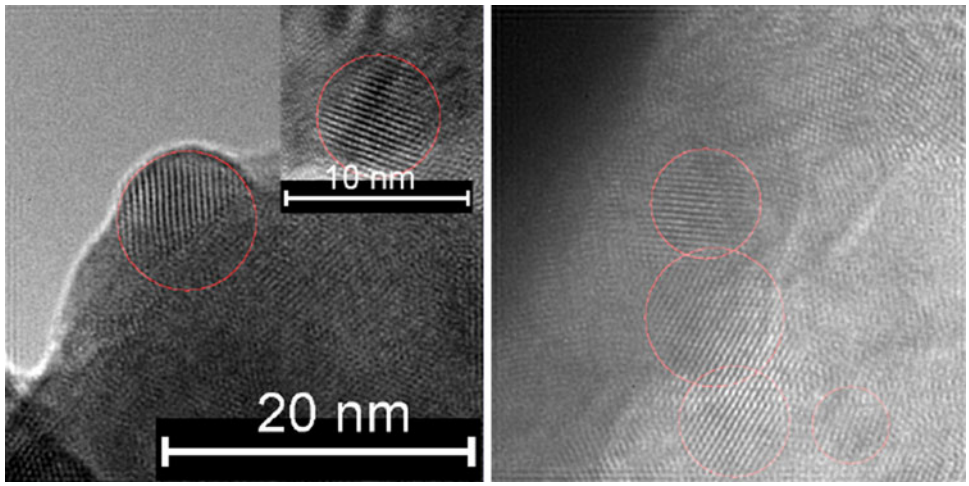


Fig. 3. HRTEM images of small $CdTe_{0.5}Se_{0.5}$ nanocrystals dispersed in ethanol solution (Color figure online).

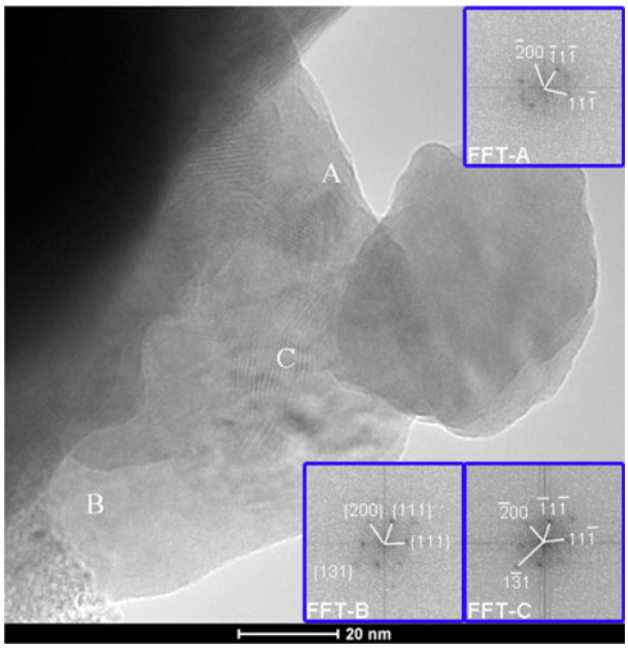


Fig. 4. HRTEM images of aggregated $CdSe_{0.5}Te_{0.5}$ nanocrystals.

($x$ = 0 to 1) NCs. All five samples were milled for 40 h and thus have similar sizes and size distributions. The color of all five $CdSe_xTe_{1-x}$ powders was black. The powder samples were pressed into a round hole (ø10 mm) in a sample holder, which was then placed into the integrating sphere mounted in the UV-3600 spectrophotometer. The reflectivity of the alloyed NCs was measured through the integrating sphere. The reflectivity was then converted to absorbance by Kramers–Kronig transformation. The CdSe and CdTe samples showed optical spectra typical of semiconductors, with a steep drop in absorption at wavelengths around the bandgap energy. This reflects the intrinsic band structure of the as-milled NCs, and is similar to the absorption spectra of bulk semiconductors, in accordance with literature reports and our previous research.[37,38,40] The alloyed $CdSe_{0.25}Te_{0.75}$, $CdSe_{0.5}Te_{0.5}$, and $CdSe_{0.75}Te_{0.25}$ samples, however, showed very different optical properties: no clear absorption band edge was observed, and strong absorption extended beyond 1400 nm. As the percentage of selenium in the $CdSe_xTe_{1-x}$ NCs increased, absorbance in the NIR range increased. It is known that both bulk CdSeTe alloys and chemically prepared CdSeTe QDs with wurtzite crystal structure exhibit a nonlinear relationship between bandgap energy and composition, called optical bowing, and it has been reported that the bandgap of CdSeTe alloys can be substantially lower than those of both binary CdSe and CdTe.[42] The optical bowing effect has been attributed to local structural ordering which arises due to differences in the ionic size, electronegativity, and lattice constants of different alloyed components. While a similar mechanism may apply in our ball-milled systems, our ball-milled samples show some distinct, unique, and previously unseen features: first, absorption extends to much longer wavelengths; second, there is no clear band edge, and the spectrum resembles those of indirect semiconductors;[43,44] third, the absorbance in the NIR range continues to increase when the Se content is as high as 75%. It is apparent that local structural ordering, or more broadly the theoretical model developed by Zunger and coworkers[45] on the observed bowing effect, is not sufficient to account for the unprecedentedly strong and broad NIR absorption of our ball-milled samples.

To gain insight into the unusual NIR absorption of the ball-milled alloys, their Raman spectra were collected. As shown in Fig. 6, longitudinal optical (LO) and transverse optical (TO) phonons, labeled as $LO_1$/$TO_1$ for CdTe-like and $LO_2$/$TO_2$ for CdSe-like, were observed between 130 $cm^{-1}$ and 220 $cm^{-1}$. The peaks between 330 $cm^{-1}$ and 430 $cm^{-1}$ correspond to second-order LO phonons. Similar to bulk CdSeTe

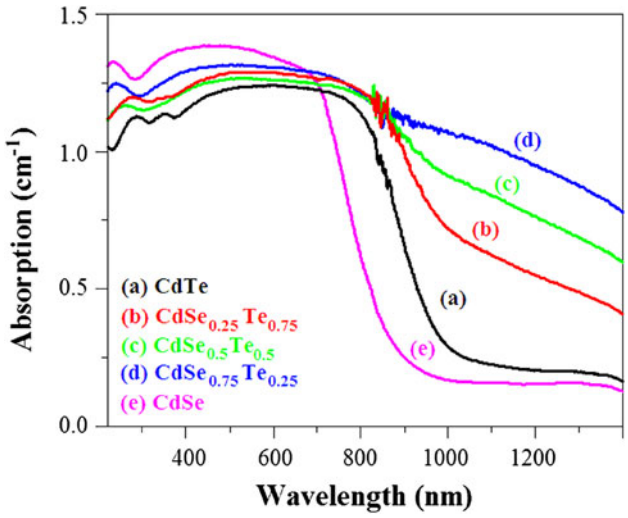


Fig. 5. UV–Vis absorption spectra of uncapped $CdSe_xTe_{1-x}$ nanocrystals.

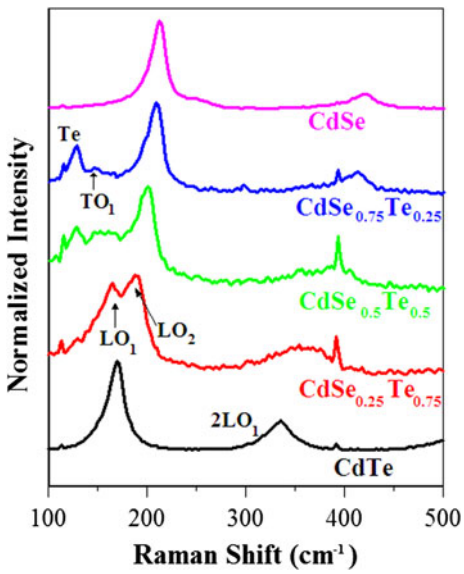


Fig. 6. Raman spectra of $CdSe_xTe_{1-x}$ ($x$ = 0 to 1) nanocrystals.

samples, the Raman spectra of ball-milled $CdSe_xTe_{1-x}$ ($x$ = 0.25, 0.5, 0.75) alloys showed both $LO_1$ and $LO_2$ bands,[46] indicating coexistence of two components. As the percentage of Se in the CdSeTe NCs increased, the intensity of the $LO_1$ peaks decreased while the $LO_2$ peaks gradually became dominant. Meanwhile, a clear Te vibrational peak at 122 cm$^{-1}$ was observed in the as-milled $CdSe_xTe_{1-x}$ ($x$ = 0.25, 0.5, 0.75) samples.[47] The intensity of this peak increased when the content of Se in the $CdSe_xTe_{1-x}$ NCs increased. These results indicate the existence of a small amount of tellurium metal in the three alloyed $CdSe_xTe_{1-x}$ samples, in accordance with the XRD results.

To find out whether Te metal clusters were present as $CdSe_xTe_{1-x}$ crystal defects, or as an

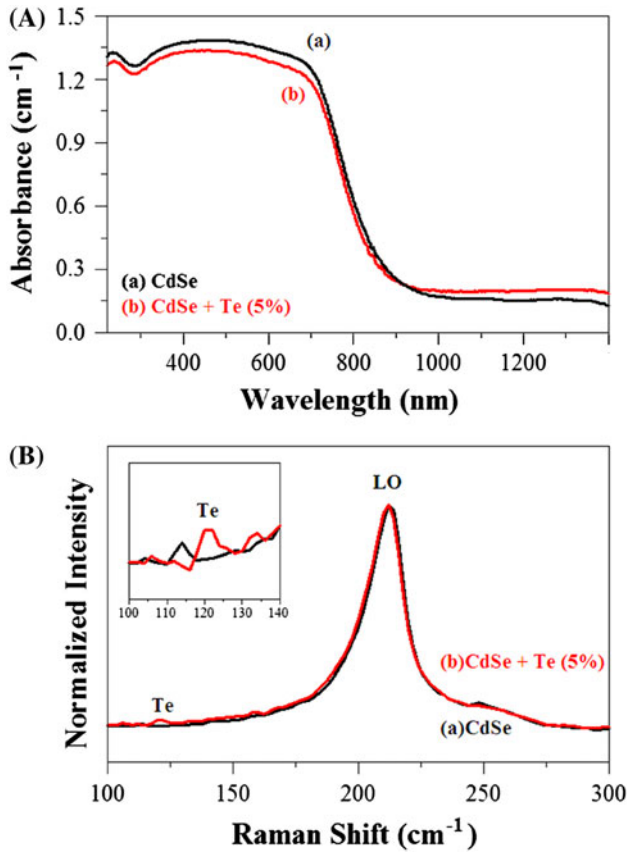


Fig. 7. (A) UV–Vis–NIR absorption and (B) Raman spectra of (a) pure CdSe NCs and (b) a physical mixture of CdSe NCs and 5% Te metal.

independent component in a physical mixture, UV–Vis–NIR absorption and Raman spectra of a physical mixture containing ball-milled CdSe NCs and 5% Te metal were measured and are shown in Fig. 7. Unlike ball-milled ternary CdSeTe samples, the physical mixture of CdSe/Te showed no NIR absorption, which indicates at least indirectly that the strong NIR absorption of the three alloyed samples is not due to the existence of Te metal as a physical mixture, but rather as defects of the $CdSe_xTe_{1-x}$ crystals. It has been reported that a small amount of Te impurity in bulk CdTe can lead to rather strong defect bands which are lower in energy than the bound excitons.[47] We believe that defect bands arising from local Te clusters are the major contributor to the ternary alloys' NIR absorption, although the regular optical bowing mechanism may play a role as well.

## CONCLUSIONS

Homogeneous $CdSe_xTe_{1-x}$ ($x$ = 0 to 1) NCs have been prepared by HEBM. By changing the initial loading of the Cd, Se, and Te elemental reactants, various ternary NCs with different chemical compositions could be obtained. The mechanochemical reaction of the elemental reactants was completed

in 5 h, as confirmed by x-ray diffraction measurements. HRTEM studies showed that the average size of the as-prepared $CdSe_{0.5}Te_{0.5}$ NCs was $<10$ nm. FFT of several individual $CdSe_{0.5}Te_{0.5}$ NCs showed that the crystalline structure was dominated by the fcc zincblende structure. The crystalline lattice parameters decreased linearly as the molar ratio of Se increased. Although as-milled CdSe and CdTe NCs show typical optical behavior of direct semiconductors, the ternary $CdSe_{0.25}Te_{0.75}$, $CdSe_{0.5}Te_{0.5}$, and $CdSe_{0.75}Te_{0.25}$ NCs showed strong absorption in the NIR range, presumably due to both the optical bowing effect and Te-induced crystal defects, as confirmed by Raman spectroscopy. Such ternary NCs are appealing materials for application in NIR-sensitive photodetectors.

## ACKNOWLEDGEMENTS

We thank the National Science Foundation (DMR 0804158) and the Army Research Office (W911NF-10-1-0476) for support of this work.

## REFERENCES

1. M. Bruchez, M. Moronne, P. Gin, S. Weiss, and A.-P. Alivisatos, *Science* 281, 2013 (1998).
2. W.-C.-W. Chan and S.-M. Nie, *Science* 281, 2016 (1998).
3. S.-W. Kim, J.-P. Zimmer, S. Ohnishi, J.-B. Tracy, J.-V. Frangioni, and M.-G. Bawendi, *J. Am. Chem. Soc.* 127, 10526 (2005).
4. N.-C. Greenham, X. Peng, and A.-P. Alivisatos, *Phys. Rev. B* 54, 17628 (1996).
5. K.-S. Leschkies, R. Divakar, J. Basu, E. Enache-Pommer, J.-E. Boercker, C.-B. Carter, U.-R. Kortshagen, D.-J. Norris, and E.-S. Aydil, *Nano Lett.* 7, 1793 (2007).
6. I. Robel, V. Subramanian, M. Kuno, and P.-V. Kamat, *J. Am. Chem. Soc.* 128, 2385 (2006).
7. M.-G. Panthani, V. Akhavan, B. Goodfellow, J.-P. Schmidtke, L. Dunn, A. Dodabalapur, P.-F. Barbara, and B.-A. Korgel, *J. Am. Chem. Soc.* 130, 16770 (2008).
8. D. Beydoun, R. Amal, G. Low, and S. McEvoy, *J. Nanopart. Res.* 1, 439 (1999).
9. X.-B. Chen, L. Liu, P.-Y. Yu, and S.-S. Mao, *Science* 331, 746 (2011).
10. V.-L. Colvin, M.-C. Schlamp, and A.-P. Alivisatos, *Nature* 370, 354 (1994).
11. A.-H. Mueller, M.-A. Petruska, M. Achermann, D.-J. Werder, E.-A. Akhadov, D.-D. Koleske, M.-A. Hoffbauer, and V.-I. Klimov, *Nano Lett.* 5, 1039 (2005).
12. M.-Y. Gao, C. Lesser, S. Kirstein, H. Möhwald, A-L. Rogach, and H. Weller, *J. Appl. Phys.* 87, 2297 (2000).
13. Z. Deng, H. Yan, and Y. Liu, *J. Am. Chem. Soc.* 131, 17744 (2009).
14. Y.-A. Yang, H.-M. Wu, K.-R. Williams, and Y.-C. Cao, *Angew. Chem. Int. Ed. Engl.* 44, 6712 (2005).
15. M.-A. Hines and P.-G. Sionnest, *J. Phys. Chem.* 100, 468 (1996).
16. W.-K. Bae, M.-K. Nam, K. Char, and S. Lee, *Chem. Mater.* 20, 5307 (2008).
17. W.-L. Jia, E.-P. Douglas, F. Guo, and W.-F. Sun, *Appl. Phys. Lett.* 85, 6326 (2004).
18. L.-Y. Wang, J.-W. Bai, Y.-J. Li, and Y. Huang, *Angew. Chem. Int. Ed. Engl.* 47, 2439 (2008).
19. W. Jiang, A. Singhal, J. Zheng, C. Wang, and W.-C.-W. Chan, *Chem. Mater.* 18, 4845 (2006).
20. T. Pons, N. Lequex, B. Mahler, S. Sasnouski, A. Fragola, and B. Dubertret, *Chem. Mater.* 21, 1418 (2009).
21. B. Dubertret, P. Skourides, D.-J. Norris, V. Noireaux, A.-H. Brivanlou, and A. Libchaber, *Science* 298, 1759 (2002).
22. X. Michalet, F.-F. Pinaud, L.-A. Bentolila, J.-M. Tsay, S. Doose, J.-J. Li, G. Sundaresan, A.-M. Wu, S.-S. Gambhir, and S. Weiss, *Science* 307, 538 (2005).
23. T. Kawano, Y. Niidome, T. Mori, Y. Katayama, and T. Niidome, *Bioconjugate Chem.* 20, 209 (2009).
24. P.-K. Jain, I.-H. El-Sayed, and M.-A. El-Sayed, *Nano Today* 2, 18 (2007).
25. R. Weissleder, *Nat. Biotechnol.* 19, 316 (2001).
26. H. Du, C.-L. Chen, R. Krishnan, T.-D. Krauss, J.-M. Harbold, F.-W. Wise, M.-G. Thomas, and J. Silcox, *Nano Lett.* 2, 1321 (2002).
27. A. Lipovskii, E. Kolobkova, V. Petrikov, I. Kang, A. Olkhovets, T. Krauss, M. Thomas, J. Silcox, F. Wise, Q. Shen, and S. Kycia, *Appl. Phys. Lett.* 71, 3406 (1997).
28. N. Goswami, A. Giri, S. Kar, M.-S. Bootharaju, R. John, P.-L. Xavier, T. Pradeep, and S.-K. Pal, *Small* 8, 3175 (2012).
29. H. Takeda and K. Adachi, *J. Am. Ceram. Soc.* 90, 4059–4061 (2007).
30. C. Kittel, *Introduction to Solid State Physics* (New York: Wiley, 1986), p. 185.
31. R.-B. Wang, O. Calvignanello, C.-I. Ratcliffe, X.-H. Wu, D.-M. Leek, M.-B. Zaman, D. Kingston, J.-A. Ripmeester, and K. Yu, *J. Phys. Chem. C* 113, 3402 (2009).
32. F.-F. Cheng, G.-X. Liang, Y.-Y. Shen, R.-K. Rana, and J.-J. Zhu, *Analyst* 138, 666 (2012).
33. Y.-C. Cao and J.-H. Wang, *J. Am. Chem. Soc.* 126, 14336 (2004).
34. I.-J. Lin and S. Nadiv, *Mater. Sci. Eng.* 39, 193 (1979).
35. P.-G. McCormick, T. Tsuzuki, J.-S. Robinson, and J. Ding, *Adv. Mater.* 13, 1008 (2001).
36. P. Baláž, P. Pourghahramani, M. Achimovičová, E. Dutková, J. Kováč, A. Šatka, and J.-Z. Jiang, *J. Cryst. Growth* 332, 1 (2011).
37. G.-L. Tan, J.-H. Du, and Q.-J. Zhang, *J. Alloys Compd.* 468, 421 (2009).
38. G.-L. Tan, N. Wu, J.-G. Zheng, U. Hommerich, and D. Temple, *J. Phys. Chem. B* 110, 2125 (2006).
39. S. Patra, B. Satpati, and S.K. Pradhan, *J. Appl. Phys.* 106, 034313 (2009).
40. G.-L. Tan, S.-H. Li, J.-B. Murowchick, C. Wisner, N. Leventis, and Z.-H. Peng, *J. Appl. Phys.* 110, 124306 (2011).
41. R. Krishnan, W.-K. Kim, E.-A. Payzant, Y. Sohn, B. Yao, and T.-J. Anderson, *37th IEEE Photovoltaic Specialists Conference (PVSC)* (Piscataway: IEEE, 2011), p. 000393.
42. R.-E. Bailey and S. Nie, *J. Am. Chem. Soc.* 125, 7100 (2003).
43. J.-J. Chen, W.-H. Tang, L.-P. Xin, and Q. Shi, *Appl. Phys. A* 102, 213 (2011).
44. K. Bindu, J. Campos, M.-T. Nair, A. Sánchez, and P.-K. Nair, *Semicond. Sci. Technol.* 20, 496 (2005).
45. S.-H. Wei, S.-B. Zhang, and A.-J. Zunger, *J. Appl. Phys.* 87, 1304 (2000).
46. Z.-C. Feng, P. Becla, L.-S. Kim, S. Perkowitz, Y.-P. Feng, H.-C. Poon, K.-P. Williams, and G.-D. Pitt, *J. Cryst. Growth* 138, 239 (1994).
47. M. Levy, N. Amir, E. Khanin, Y. Nemirovsky, and R. Beserman, *J. Cryst. Growth* 197, 626 (1999).